Earthq Eng & Eng Vib (2020) 19: 87-104 **DOI**: https://doi.org/10.1007/s11803-020-0549-y

Field measurements for calibration of simplified models of the stiffening effect of infill masonry walls in high-rise RC framed and shear-wall buildings

Zhou Yun[1, 2, 3†], Pei Yilin[1‡], Zhou Yi[1§], Hyeon-Jong Hwang[1*] and Yi Weijian[1†]

1. *College of Civil Engineering, Hunan University, Changsha 410082, China*
2. *Hunan Provincial Key Lab on Damage Diagnosis for Engineering Structures, Hunan University, Changsha 410082, China*
3. *Key Laboratory for Green & Advanced Civil Engineering Materials and Application Technology of Hunan Province, Hunan University, Changsha 410082, China*

Abstract: As a type of nonstructural component, infill walls play a significant role in the seismic behavior of high-rise buildings. However, the stiffness of the infill wall is generally either ignored or considered by simplified empirical criteria that lead to a period shortening. The difference can be greatly decreased by using a structural identification methodology. In this study, an ambient vibration test was performed on four on-site reinforced concrete high-rise buildings, and the design results were compared with the PKPM models using corresponding finite element (FE) models. A diagonal strut model was used to simulate the behavior of the infill wall, and the identified modal parameters measured from the on-site test were employed to calibrate the parameters of the diagonal strut in the FE models. The SAP2000 models with calibrated elastic modulus were used to evaluate the seismic response in the elastic state. Based on the load-displacement relationship of the infill wall, nonlinear dynamic analysis models were built in PERFORM-3D and calibrated using the measured modal periods. The analysis results revealed that the structural performance under small/large earthquake records were both strengthened by infill walls, and the contribution of infill walls should be considered for better accuracy in the design process.

Keywords: high-rise building; ambient vibration test; model calibration; infill wall; seismic performance; nonlinear dynamic analysis

1 Introduction

Due to widely used lightweight materials, high-rise buildings have become more flexible and thus more sensitive to external excitations. As a type of horizontal load, seismic action is critical to high-rise building design. The seismic response is affected by nonstructural components including infill walls, which has been concluded from previous substantial earthquake disasters. The use of masonry infill walls significantly increases the initial stiffness of building structures, but abrupt stiffness degradation occurs after the infill walls are damaged (Chaulagain *et al*., 2016; Dhakal *et al*., 2016). Furthermore, the irregular and unreasonable arrangement of the infill wall may also induce an adverse effect on the structural responses (e.g., torsion effect, short-column effect, and weak layer failure). However, the contribution of the infill wall to the stiffness is generally ignored in the seismic design of building structures (Sanada and Konishi, 2011). To consider the structural performance influenced by the stiffness of the infill wall, a natural period reduction factor is recommended in current design codes (Kaushik *et al*., 2012). Chinese design code JGJ 3-2010 (2010) specifies the factor of 0.7 to 1.0, and the Canadian design code (NRCC, 2005) specifies 0.8. Moreover, a series of specific formulas is utilized to estimate the natural period of reinforced concrete (RC) frames with infill walls (Zhou *et al*., 2017).

The installation of infill walls decreases the natural period of structures, which can be measured from an on-site ambient vibration test (Li and Wu, 2004). The ambient vibration test in high-rise buildings exhibits a large difference of the fundamental frequency between the predictions and actual measured records due to improper modeling approaches of nonstructural components (Li *et al*., 2004, 2010). The seismic capacity of high-rise

Correspondence to: Zhou Yun, College of Civil Engineering, Hunan University, Changsha 410082, China
Tel: +86-18684920470
E-mail: zhouyun05@hnu.edu.cn
†Professor; ‡Postgraduate Student; §Master; *Associate professor

Supported by: National Key Research and Development Program of China under Grant Nos. 2016YFC0701400 and 2016YFC0701308, the Key Research and Development Program of Hunan Province under Grant No. 2017SK2220, and the National Natural Science Foundation of China (NSFC) under Grant No. 51878264
Received September 8, 2018; **Accepted** May 27, 2019

buildings is affected by the dynamic characteristics related to the mass and stiffness distributions. Thus, the mass and stiffness of the infill walls should be considered in the evaluation of the seismic capacity.

The structural identification (St-Id) method, proposed by Liu and Yao (1978), is a systematic approach for characterizing the structural behavior of an unknown system on the basis of the input and output test data. St-Id was summarized as a six-step analysis-test-decision integration cycle by ASCE St-Id of Constructed Systems Committee as follows (ASCE, 2011): (1) Objectives, observation, and conceptualization; (2) A priori finite element (FE) modeling; (3) Uncontrolled and controlled tests; (4) Processing, validation, and interpretation of data; (5) Model calibration and parameter identification; and (6) Utilization of the calibrated model for simulation and decision-making. Over the last few decades, the state of the art in St-Id of constructed systems has advanced significantly, and dozens of successful applications for structural systems have been documented (Catbas *et al*., 2013).

The identified dynamic characteristics obtained from an on-site test can be employed to update the related parameters of the FE model (Brownjohn, 2003). The measurement of the structural dynamic response from ambient vibration tests, such as microtremors, wind vibration, and traffic vibration, is increasingly important to obtain the fundamental period of high-rise buildings. Based on the on-site test record, the FE model can be calibrated to minimize the difference between the predictions and measured dynamic characteristics, and the calibrated FE model is applicable to structural analysis (Xu *et al*., 2003). Other applications mainly include structural health monitoring, seismic vulnerability evaluation, and vibration control (Brownjohn and Pan, 2008).

Uncertainty in the modeling of infill walls was introduced in an a priori FE model of high-rise buildings, which was generally utilized to estimate modal information before implementing the ambient excitation test for an actual structure. The current computational models to simulate the mechanical behavior of the infill wall are broadly divided into FE micro-model and macro-model. In the micro-model, the infill wall is considered as a continuous element addressing local details, and the material properties of the mortar, brick, and other constituent elements can be built. The FE micro-model is generally regarded as the most precise analysis method for infill wall modeling (Hans *et al*., 2010), although considerable calculation time is required (Asteris *et al*., 2013). The macro-model can be developed based on the observed seismic behavior and test results (Asteris *et al*., 2011). According to Polyakov (1960), an infill wall can be converted into a diagonal strut within its panel. Holmes (1961) further improved a simplified model with an equivalent pin-jointed diagonal strut. Smith (1962) presented a mathematical equation to estimate the equivalent width of the diagonal strut. Mainstone (1971) proposed an empirical equation for the equivalent strut width based on test results, which was simultaneously included in FEMA-274 (1997) and FEMA-306 (1999) guidelines and has been widely used in the analysis of RC frames with infill walls (Fardis and Panagiotakos, 1997; Negro and Colombo, 1997; Balendra and Huang, 2003). Eurocode 8 (2004) prescribes the detailed arrangement of the infill wall at the first story, but the calculation procedure is relatively complicated in the design procedure.

Based on Chinese seismic design code GB 50011-2010 (2010), mode-superposition response spectrum analysis and linear dynamic analysis are applied to the structural analysis under small earthquakes. Under large earthquakes, the pushover analysis method and nonlinear dynamic analysis are used to consider plastic behavior. A similar analytical procedure is adopted in Eurocode 8 (2004) and American design codes (ASCE, 2006), although these codes differ in the selection of the site category, seismic grouping, and structural vibration period.

The dynamic characteristics of the RC frame structures with infill walls have also been widely discussed. Henderson *et al.* (2003) demonstrated that an actual masonry infill wall can resist lateral load more effectively than suggested by the design code procedures. Su *et al*. (2005) indicated that nonstructural components significantly increase the global lateral stiffness of structures. Hashmi and Madan (2008) reported that an infill wall decreases the lateral deformation and damage of frame structures. According to Kose and Karslioglu (2010), the use of infill walls decreases the first mode period of structures and increases the spectral acceleration coefficient in response analysis. Zhang *et al.* (2011) performed numerical analysis to investigate the effect of infill walls on the failure pattern of RC frames, and reported that the infill effect needs to be considered in structural design. Nautiyal *et al.* (2013) found that the base shear of a four-story frame is increased by an infill wall in the equivalent diagonal strut method. Su and Lee (2013) proposed a coefficient-based method for the seismic fragility analysis and ultimate spectral displacement assessment of RC buildings using infill walls, which is applicable to both the performance evaluation of existing buildings and conceptual design of new buildings. Nwofor and Chinwah (2014) discovered that the shear strength of a building structure with infill walls decreases with an increase of the opening ratio of the infill walls. Luis *et al.* (2014) reported that the openings at the corner of infill walls decrease the strength and stiffness of the infilled frames, which should not be used in high-seismicity regions. Ashok *et al.* (2015) observed that an infill wall increases the seismic resistance of frame structures. Al-Nimry *et al.* (2015) conducted nonlinear static analysis of 112 low-rise and medium-rise buildings with infill walls, and found that approximately 40% of the existing buildings require detailed analysis to better evaluate their seismic

vulnerabilities. Milheiro *et al.* (2016) recommended that nonlinear analysis be performed to consider the infill wall contribution to the design of new buildings and the evaluation of the seismic performance of existing buildings. Abhijeet and Vaibhav (2017) observed that the maximum deflection and story drift ratio are restricted in high-rise buildings with infill walls and outrigger systems.

The core ideology of the St-Id approach lies in the estimation of the structural response performed by the calibrated FE model. The discrepancy between the seismic analysis result of high-rise buildings and actual structural behavior is mainly caused by the uncertainty of the modeling process (particularly, the effect of nonstructural components, such as infill walls, is neglected). Although the uncalibrated FE model without consideration of infill walls is generally used in seismic analysis, the difference in seismic performance between the uncalibrated and calibrated FE model has seldom been studied. In the present study, the FE model was calibrated by using the actual period measured from the ambient vibration test, and the structural performance was evaluated by the calibrated FE models. The mode-superposition response spectrum analysis method and nonlinear dynamic analysis method were adopted to evaluate the elastic behavior under small earthquakes and plastic behavior under large earthquakes, respectively. Figure 1 shows the detailed procedure. The effect of an infill wall on the seismic performance of structures was discussed, and the seismic analysis results calculated by the calibrated model and uncalibrated model were carefully compared.

2 On-site tests of Laibin high-rise buildings

Target buildings were tested in downtown Laibin in Guangxi, China. Ten residential RC buildings with heights of approximately 100 meters were carefully selected from more than 200 high-rise buildings. The infill wall of the structures was built by brick masonry and cement mortar. To achieve a convenient and scientific comparison, four representative high-rise buildings (BAYG 2#, JSXQ 3#, XYY A#, and SHHM 2#) were selected from each residential region for dynamic testing. The heights of BAYG 2#, JSXQ 3#, XYY A#, and SHHM 2# were 87.0 m with 26 stories, 122.7 m with 39 stories, 86.1 m with 24 stories, and 107.4 m with 33 stories, respectively. Figure 2 shows the building information and instrumentation layout. BAYG 2# is a frame-shear wall structure, and the other three buildings are shear wall structures. Twelve kinds of beam sections (section range 150 mm × 300 mm–300 mm × 800 mm) were used, and the majority of the column section was about 500 mm × 500 mm (section range 350 mm × 400 mm–700mm × 700 mm). In BAYG 2#, JSXQ 3#, XYY A#, and SHHM 2#, the total number of infill wall panels was 86, 104, 118, and 76 in each story, and the thickness of the infill wall was 220 mm, 180 mm, 270 mm, and 300 mm, respectively. The thickness of the RC walls was 240 mm–500 mm. The infill wall was constructed by MU10 porous shale bricks combined with M5 cement mortar, and the corresponding masonry compressive strength was 2.4 MPa and Poisson's ratio was 0.2. The tested structures were built at the same construction site where the soil type was limestone with plain fills, and supported by piles with man-excavated shaft. The field category was classified as class 2, and the seismic intensity was classified as degree 6 according to Chinese design code GB 50011-2010. Other detailed test information can be found in the study of Zhou *et al.* (2017).

In this study, the stochastic subspace identification method (SSI) was used to analyze the signals measured from the ambient vibration test (Peeters, 2000). For

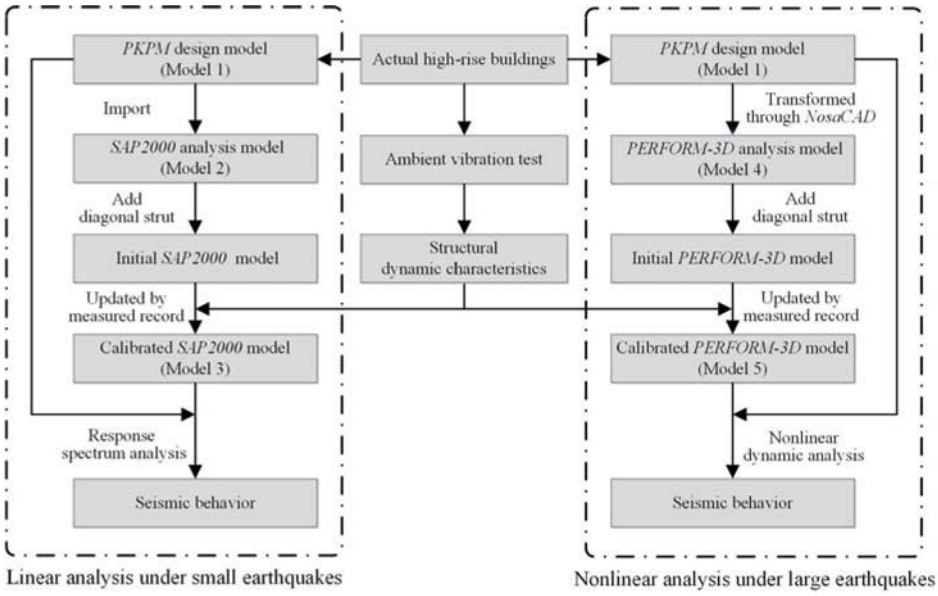

Fig. 1 Flowchart of two-stage seismic analysis for high-rise buildings

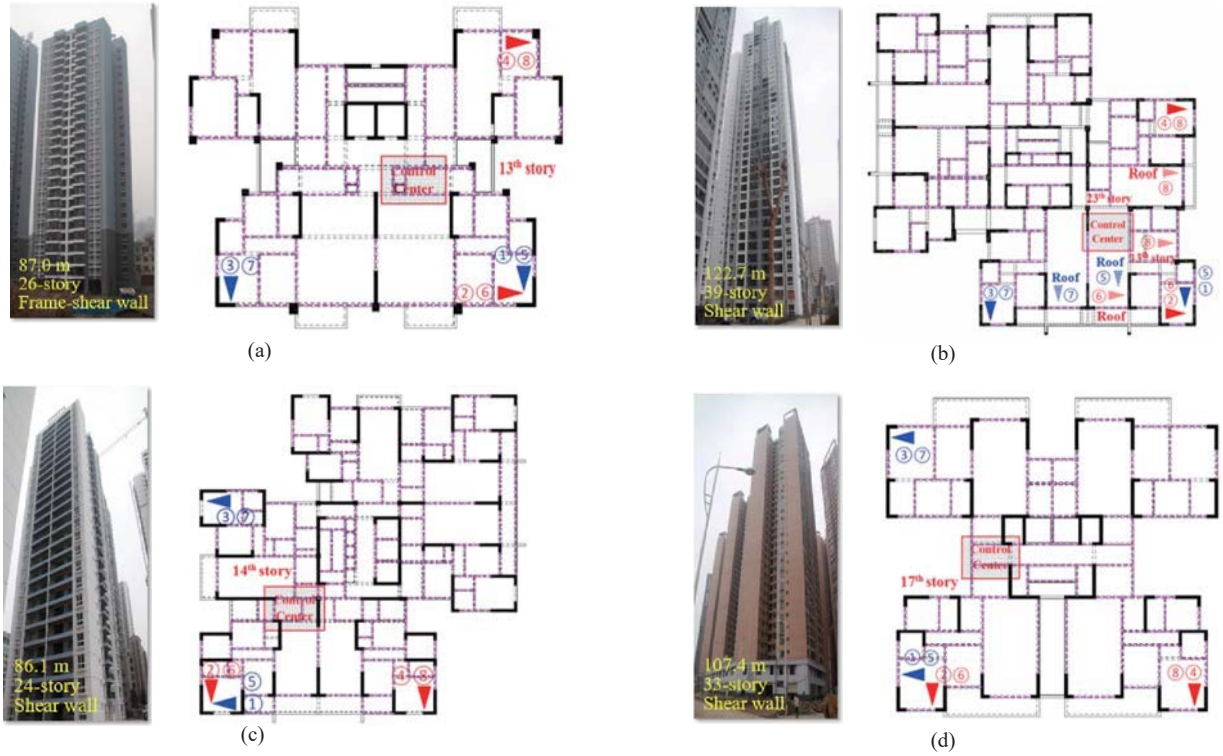

Fig. 2 Floor plan of four high-rise buildings: (a) BAYG 2#; (b) JSXQ 3#; (c) XYY A#; (d) SHHM 2# (dotted pink line indicates the infill wall)

structural design, PKPM software only considers the equivalent mass of infill walls, while the corresponding stiffness is ignored. Table 1 compares the first three periods calculated by the SATWE module in PKPM with the measurements to identify the differences. The ratio of the measured period to prediction ranged from 0.339 to 0.450 when the period reduction coefficients specified in Chinese design code JGJ 3-2010 were used (i.e., 0.7 to 0.8 for frame-shear wall structures, and 0.8 to 1.0 for shear wall structures). Figure 3 compares the calculated mode shapes with the measurements in building JSXQ 3#, demonstrating similar behavior.

3 Elastic FE model for response spectrum analysis

To evaluate the linear dynamic behavior of a high-rise building, the mode-superposition response spectrum method was used according to Chinese seismic design code GB 50011-2010 (2010). The accuracy of the FE model analysis for high-rise buildings is affected by the modeling behavior of the structural components including the slab and shear wall. In the SATWE module of PKPM software, a one-dimensional element was adopted to simulate the structural performance of the column, beam, and diagonal strut (Tan *et al*., 2015). The shear wall was simulated by the general shell element, and the slab could be assumed to have infinite stiffness or simulated by elastic theory. As general FE analysis software, SAP2000 employs frame elements to describe the behavior of the beam and column, and the shell element with membrane characteristics was adopted for the slab and shear wall in three-dimensional structures (Mwafy *et al*., 2006).

Table 1 Calculated and measured natural periods of the four buildings

Buildings	T/T coefficient	Items	1st mode (s)	2nd mode (s)	3rd mode (s)
BAYG 2#	0.74	Measured	1.245	1.122	0.958
		Calculated	3.584	3.311	2.651
JSXQ 3#	0.93	Measured	1.621	1.479	1.287
		Calculated	3.605	3.487	3.344
XYY A#	0.78	Measured	0.917	0.865	0.800
		Calculated	2.297	1.970	1.875
SHHM 2#	0.85	Measured	1.433	1.294	1.214
		Calculated	3.722	3.702	3.168

Note: T/T coefficient denotes the calculated torsion period divided by the translation period

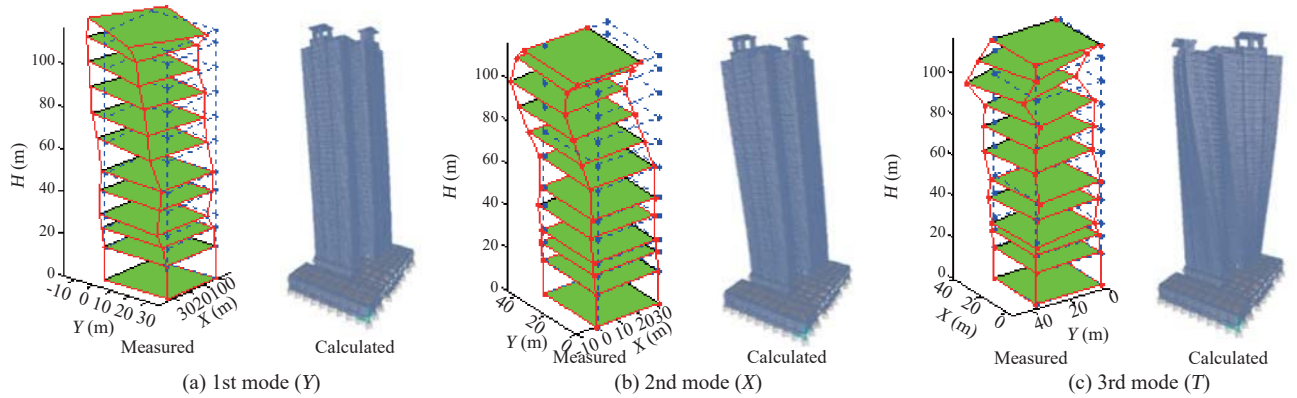

Fig. 3 Comparison between the measured and calculated modes in building JSXQ 3# (Note: *X*/*Y* denotes the *X*/*Y* direction lateral swaying mode, *T* denotes the torsional mode)

The high-rise building model was built in the SATWE module of PKPM before transferring it to SAP2000. First, the accuracy and calculation errors of the models built in SAP2000 and PKPM should be estimated, and the identical modeling strategy was adopted for each modeling. The beam element was employed for the beam and column, and the thin-shell element was adopted to simulate the behavior of the shear wall and floor slab. As shown in Fig. 4, a pair of equivalent diagonal struts that resist compression force only was used to simulate an infill panel (Paulay and Priestley, 1992; Furtado *et al*., 2015). The diagonal strut model provides sufficient accuracy to represent the major characteristics of the load-displacement relationship of the infill wall. The mechanical properties, such as initial stiffness, can be extracted from the curve. A constant thickness of the diagonal strut was assumed in each story. Similar to the modeling strategy in PKPM, the mass of the infill wall was converted into dead load, and then imposed on the corresponding beam. The density of the diagonal strut was set to zero. The complete quadratic combination (CQC) calculation method was employed to consider the structural torsional effect.

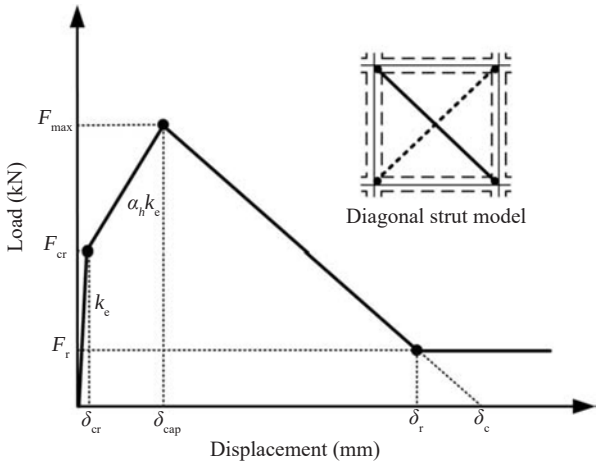

Fig. 4 Load-displacement relationship of a diagonal strut for infill walls

3.1 Initial stiffness of diagonal strut for infill walls

Strut width ω is the key parameter of the diagonal strut in FE analysis, which was proposed by Mainstone (1971), as follows:

$$\omega=0.175\lambda_h^{-0.4}d \tag{1}$$

where λ_h is the dimensionless parameter that reflects the relative stiffness of the infill wall; and d is the diagonal length of the panel.

λ_h can be calculated as follows:

$$\lambda_h = h\left(\frac{E_m t\sin(2\theta)}{4EIh'}\right)^{0.25} \tag{2}$$

where E_m, t, and h' are the elastic modulus, thickness, and height of the infill wall, respectively; θ is the angle between the diagonal strut and beam; E is the elastic modulus of the frame materials; and h and I are the height and moment inertia of the column, respectively.

The initial stiffness k_e of the infill wall is defined as follows:

$$k_e = 2\frac{E_m\omega t}{L}(\cos\theta)^2 \tag{3}$$

where L is the length of the equivalent diagonal strut.

3.2 Model verification for response spectrum analysis

Table 2 shows the types of FE models for the four selected high-rise buildings. Model 1 indicates the PKPM design model, Model 2 indicates the SAP2000 analysis model for comparison, and Model 3 adds the stiffness effect of the infill wall to Model 2. Figure 5 shows the natural periods of the first 12 modes calculated by Model 1 and Model 2 of JSXQ 3#. The identical analysis results indicate that the model of SAP2000 can represent the *PKPM* model well with regard to structural design.

Table 2 Analysis models of high-rise buildings

Models	Software	Mass of the infill wall	Stiffness of the infill wall	Period reduction coefficient	Description
Model 1	PKPM	Yes	None	Yes	Design model
Model 2	SAP2000	Yes	None	None	Comparison with the PKPM model
Model 3	SAP2000	Yes	Diagonal strut	None	Response spectrum analysis
Model 4	PERFORM-3D	Yes	None	Yes	Comparison with the PKPM model
Model 5	PERFORM-3D	Yes	Diagonal strut	None	Nonlinear dynamic analysis

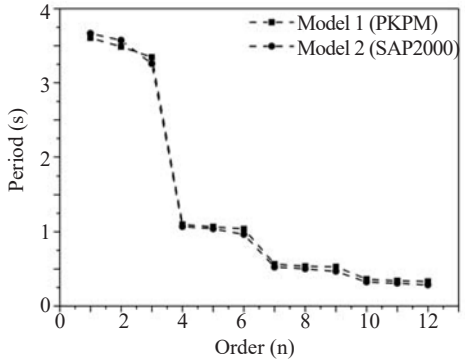

Fig. 5 Comparison of natural periods between Model 1 and Model 2 in JSXQ 3#

In Model 3 with diagonal struts, the infill wall was built using MU10 shale porous bricks and M5 cement mortar (i.e., masonry compressive strength of 2.4 MPa, and Poisson′s ratio of 0.2). According to the test report of the contractor, the initial elastic modulus of the infills was selected as 1.85×10^4 N/mm^2. Because of the large difference of modal periods between the analysis result by FE software and measurement in the building JSXQ 3#, the elastic modulus of the infill wall was modified by a trial and error analysis to 1.45×10^4 N/mm^2. As shown in Fig. 6, the modal period of JSXQ 3# predicted by the calibrated Model 3 agreed well with the measurement.

4 FE model for nonlinear dynamic analysis

In nonlinear behavior of a structure under large earthquakes, the lateral stiffness of the infill wall gradually decreases as the damage develops (Almeida *et al*., 2016). To investigate the nonlinear seismic behavior of the structure using the calibrated infill wall model, PERFORM-3D, specialized software for performance-based seismic analysis, was used (Mamun and Saatcioglu, 2017). The building models in PKPM were transformed by NosaCAD to PERFORM-3D for nonlinear dynamic analysis (Wu, 2012). The load cases in PERFORM-3D were identical to those in the SATWE module of PKPM, and a rigid floor was assumed for simple calculation.

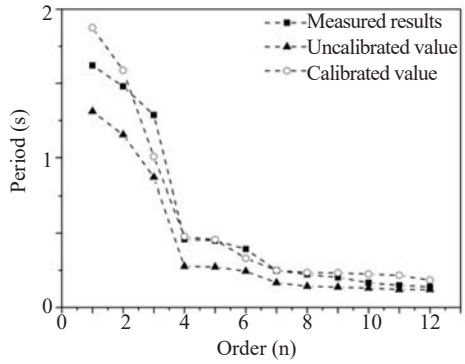

Fig. 6 Natural periods of Model 3 with/without calibration in JSXQ 3#

Beams that have relatively small axial forces, are therefore usually not necessary to account for P-M interaction, while columns with relatively large axial forces, are therefore necessary to account for P-M interaction. Thus, beams usually bend in only one plane, and it is not necessary to consider biaxial bending or biaxial shear. While columns usually bend along about both cross section axes, biaxial bending and biaxial shear need to be considered. In PERFORM-3D, the element that consists of an intermediate elastic segment and a terminal elastic-plastic segment is used to describe the nonlinear behavior of frame members. The trilinear moment-curvature hysteretic models are utilized in the elastic-plastic segment of the beam under bending moment, and the fiber model is adopted in the elastic-plastic segment to describe the nonlinear behavior of the column under moment and axial force at both ends (Epackachi *et al*., 2012). The general shear wall element developed by PERFORM-3D was used in the wall model to consider the complex stress state (Burak and Comlekoglu, 2013). The coupling beam component is simulated by the beam element with a shear hinge to describe the nonlinear shear stiffness. The diagonal strut model for the nonlinear behavior of the infill wall is considered in PERFORM-3D (Wu *et al*., 2014). Figure 7 shows the load-displacement relationship of the infill wall in PERFORM-3D. The curve *YULRX* describes the concrete behavior, and the degeneration coefficients for the energy dissipation capacity are 1.0 (point *Y*), 0.9 (point *U*), 0.7 (point *L*), 0.4 (point *R*), and 0.3 (point *X*). The trilinear curve '*YUX*' describes the behavior of reinforcing bars. Figure 7(b) shows the hysteretic curve for one masonry diagonal at the bottom story of JSXQ 3# under RSN 304 action.

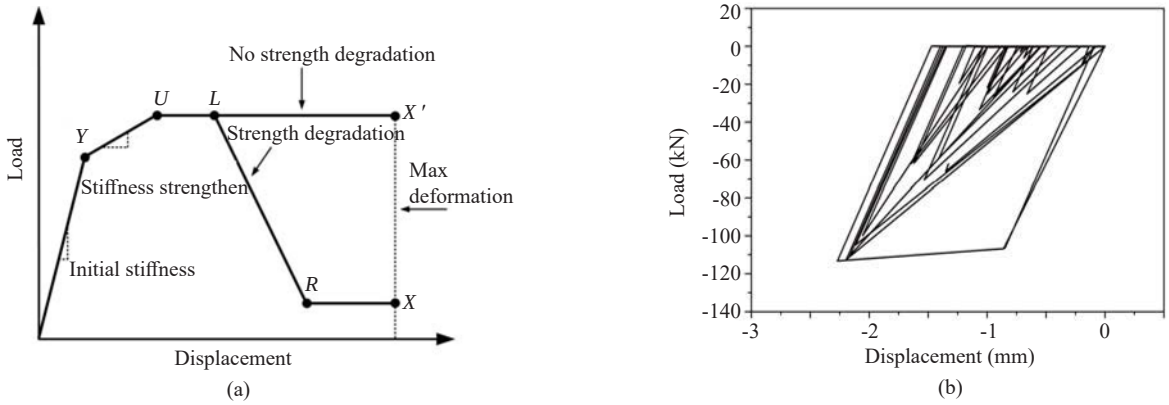

Fig. 7 Envelope performance of masonry diagonal components: (a) Load-displacement relationship; (b) Hysteretic curve of JSXQ 3# under RSN 304 action

4.1 Load-displacement relationship of infill walls

Figure 8 shows the procedure to calculate the load-displacement relationship of the infill wall. The peak strength can be determined from Eq. (4), proposed by Zarnic and Gostic (1998) and revised by Dolsek and Fajfar (2008):

$$F_{\max} = 0.818 \frac{L_{\text{in}} t f_{\text{tp}}}{C_I} (1 + \sqrt{C_I^2 + 1}) \tag{4a}$$

$$C_I = 1.925 \frac{L_{\text{in}}}{h'} \tag{4b}$$

where L_{in} is the length of the infill wall; and f_{tp} is the cracking stress of the masonry brick obtained from the diagonal compression test.

The mechanical properties including the peak strength and residual strength of the infill wall can be extracted from the load-displacement relationship of the nonlinear diagonal strut model. As shown in Fig. 4, the stiffness of the infill wall is degraded to $\alpha_h k_e$ after crack initiation. According to Manzouri (1995) and Dolsek and Fajfar (2008), the cracking strength F_{cr} of the infill wall is approximately 0.55 times the peak strength (i.e., F_{cr}=0.55$F_{\max}$). The displacement δ_{cap} corresponding to the peak strength can be approximately defined as 0.25% of the story drift ratio, on the basis of the test results performed by Manzouri (1995) and Shing *et al.* (2009). Dolsek and Fajfar (2008) suggested that the residual strength of the infill wall is 0.2 times the peak strength, and the corresponding displacement can be calculated by the displacement δ_c at zero strength. δ_c is approximately five times greater than δ_{cap} based on a series of tests implemented by Carvalho and Coelho (2001).

4.2 Model verification for nonlinear dynamic analysis

Model 4 indicates that the contribution of infill walls to structural stiffness is considered using the period reduction factor in PERFORM-3D. As shown in Fig. 9, the modal periods of JSXQ 3# calculated by PERFORM-3D are basically consistent with those of PKPM, which indicates that the PERFORM-3D analysis model is reasonable for nonlinear analysis.

In Model 5, the modeling of the diagonal strut for the infill wall is added to Model 4 (refer to Table 2). Table 3 shows the design parameters of the infill walls in JSXQ 3#. The height of the first story is approximately 3.8 m, the height of the other stories is 2.9 m, and the width of the infill wall ranges from 1 m to 5.5 m. The width ω and cross-sectional area of the diagonal strut can be calculated by Eq. (1). For C40 and C45 concrete used in the frame, the elastic modulus is defined as 3.25×10^4 N/mm^2 and 3.35×10^4 N/mm^2, respectively. Compared with the measurement from the on-site dynamic test, the initial elastic modulus of the masonry infills was re-defined as

Table 3 Diagonal strut width according to design parameters in JSXQ 3#

Height of infill wall (mm)	Width of infill wall (mm)	Width of diagonal strut (mm)	Cross-section area of diagonal strut (mm^2)	Height of infill wall (mm)	Width of infill wall (mm)	Width of diagonal strut (mm)	Cross-section area of diagonal strut (mm^2)
h = 2900	1000	337	60649	h = 3800	1000	424	76385
	2000	392	70538		2000	453	81571
	3000	482	86815		3000	518	93190
	4000	592	106474		4000	603	108505
	5000	712	128159		5000	701	126179

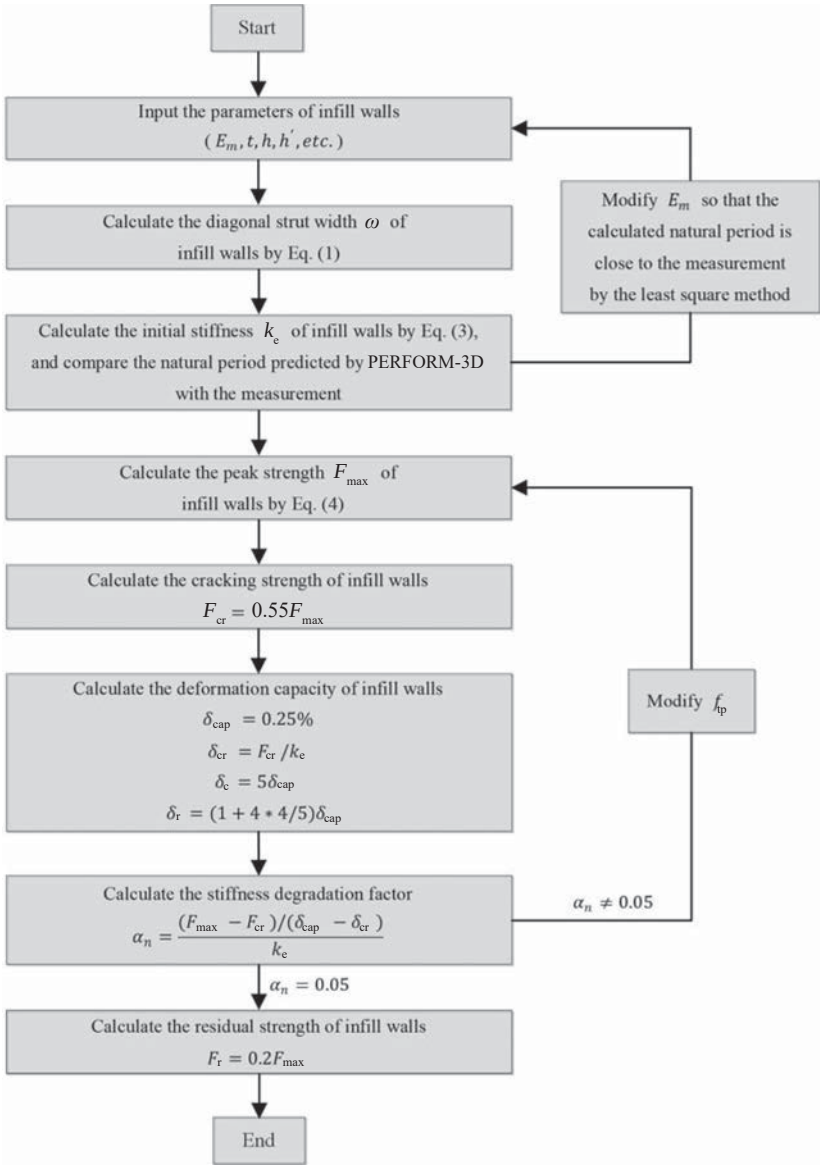

Fig. 8 Flowchart to determine the load-displacement relationship of the diagonal strut

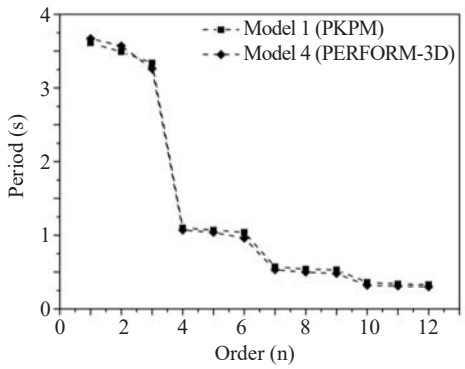

Fig. 9 Comparison of natural periods between Model 1 and Model 4 in JSXQ 3#

1.85×10^4 N/mm^2. The contribution of the infill wall to the elastic analysis model of JSXQ 3# is dependent on the elastic modulus and cross-section area.

Figure 10 compares the natural periods according to the elastic modulus of the infill wall in JSXQ 3#. Using the least squares method for the periods of the 12 modes, the optimal initial elastic modulus of the infill wall in JSXQ 3# was estimated as 1.45×10^4 N/mm^2. Modal damping of 5% and 0.2% βk damping were used in the global structure. The implicit Newmark-β calculation method was adopted to consider the actual condition of structural performance.

The envelope curve of the infill wall can be calculated using the proper elastic modulus. One of the most important coefficients is the peak stress F_{max}, which depends on the length, width, height, and cracking stress f_{tp} of the masonry infill wall according to Eq. (4). f_{tp} is usually adopted as 4% to 8% of the masonry compression strength f_c, which can be determined from Eq. (5):

$$f_c = k_1 f_1^{\alpha}(1 + 0.07 f_2) \tag{5}$$

where f_1 is the compressive strength of brick; f_2 is the

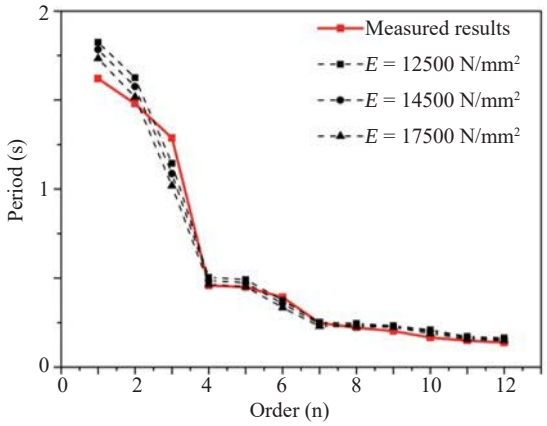

Fig. 10 Natural period variances according to the elastic modulus of infill walls in JSXQ 3#

compressive strength of mortar; and k_1, α and k_2 are the coefficients related to the type of brick specified in the design code. The reasonable range of f_{tp} can be acquired based on f_c, and the specific value of f_{tp} is determined based on the stiffness degradation coefficient α_n.

For example, the infill wall of JSXQ 3# was composed of perforated shale brick with cement mortar, and f_c was calculated as 3.3 MPa in Eq. (5). The reasonable range of f_{tp} was 0.13 MPa to 0.27 MPa (i.e., 4 to 8% of f_c), and the envelope curve of the infill wall was estimated according to the procedure in Fig. 8. Note that a 16% to 20% change of the elasticity modulus of the infill wall would generate the 15% to 35% decrease/increase of the initial stiffness in the envelope curve, and the global component performance is also affected as shown in Fig. 11. Figure 12 shows the envelope curves of the infill walls with various widths at the standard floor (h = 2.9 m) of JSXQ 3#, and f_{tp} in all cases satisfied the reasonable range of 0.13 MPa to 0.27 MPa.

5 Response spectrum analysis results under small earthquakes

5.1 Discussion of seismic influence coefficient

In the design of four high-rise buildings, field category class 2 specified in the Chinese code corresponds to the field with a mean shear wave velocity V_{30} between 260 m/s and 510 m/s in US code (Lu and Zhao, 2007). As shown in Fig. 13, the natural periods of the 1st mode in the high-rise buildings are expected to lie in the long period region of the target response spectrum, which decreases the seismic influence coefficient. The measured and calculated natural periods of the four buildings were marked in the response spectrum.

Table 4 shows the detailed information used in the response spectrum analysis. Both the PKPM and initial SAP2000 FE models overestimated the natural periods of the actual building structures because of the lack of calibration, which underestimated the seismic influence factor. After the calibration of the analysis models, the fundamental periods agreed well with the measured modal data, and then the calibrated models generated nearly the same seismic influence factor α as shown in Fig. 13. Thus, the conventional design process ignoring the stiffness effect of infill walls had the

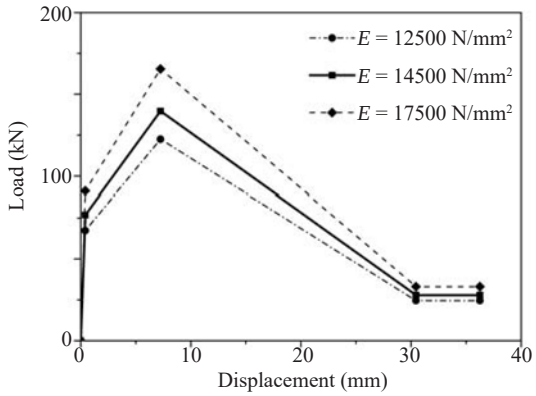

Fig. 11 Elasticity modulus adjustment of the infill wall in JSXQ 3#

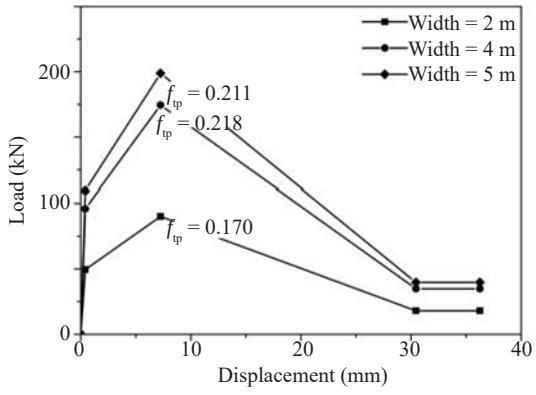

Fig. 12 Envelope curves of infill walls in JSXQ 3#

Table 4 Seismic coefficients for response spectrum analysis

Coefficient	α_{max}	η_1	η_2	γ	T_g	ζ
Value	0.04	0.02	1	0.9	0.35	0.05

Note: α_{max} denotes the maximum seismic influence coefficient, η_1 denotes the slope regulation coefficient of the linear decrease stage, η_2 denotes the damping modification factor, γ denotes the attenuation index, T_g denotes the design basic earthquake acceleration, and ζ denotes the damping ratio

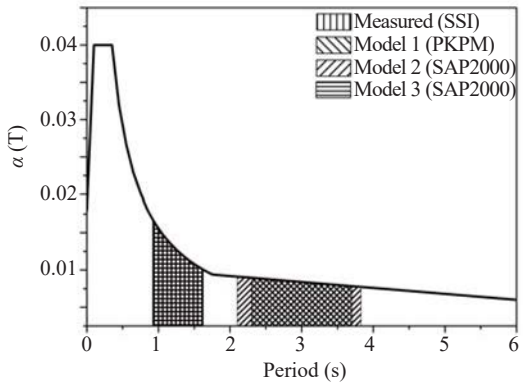

Fig. 13 Seismic influence factors in various analysis models

potential to generate an inaccurate result because of the underestimated seismic influence factor α, even when the period reduction coefficient was considered.

5.2 Inter-story shear force

Figure 14 shows the inter-story shear distributions of Model 1 and Model 3 calculated by the mode-superposition response spectrum analysis in the *X*-direction. The shear force at the bottom story of the Model 3 was approximately 1.5 to 2 times greater than that of Model 1 due to the contribution of the infill wall to the structural stiffness and resistance to seismic loading.

5.3 Inter-story drift

Figure 15 shows the story drift distributions of Model 1 and Model 3 for the four high-rise buildings. The roof displacement of Model 1 was 3 to 6 times greater than that of Model 3.

Figure 16 shows the inter-story drift ratio distributions of Model 1 and Model 3, and both values satisfied the drift requirement of the design codes. The inter-story drift ratio is defined as the maximum inter-story drift divided by the height of each floor ($\Delta u/h$), which should be less than the requirement of the structural horizontal displacement to prevent the degradation of the stability and operational performance of the structure. The maximum inter-story drift ratio of Model 1 was 3 to 6 times greater than that of Model 3.

The Chinese design code JGJ 3-2010 (2010) specifies the period reduction factor of 0.7 to 0.8 for a frame-shear structure and 0.8 to 1.0 for a shear wall structure. The Canadian design code (NRCC, 2005) specifies the coefficient for the natural frequency of 0.8 for infill structures. Although the period reduction factor was utilized in PKPM, the inter-story shear force calculated by Model 1 was approximately 0.5 times less than that of Model 3, and the horizontal drift and inter-story drift ratio of Model 1 was approximately 3 to 4 times greater than that of Model 3 (refer to Figs. 14 to 16). Thus, the recommended values need to be revised to better evaluate the shear force and drift ratio in elastic state.

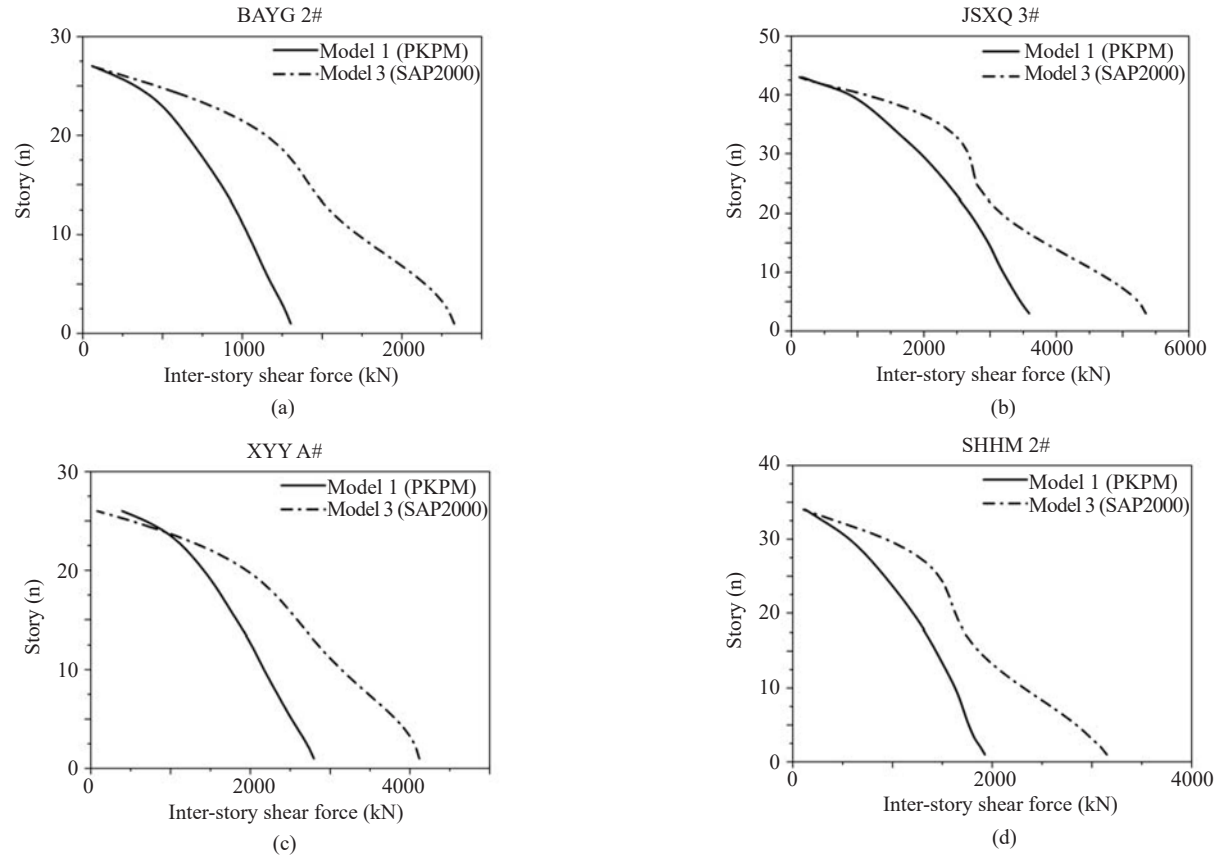

Fig. 14 Shear force distribution of buildings under small earthquakes: (a) BAYG 2#; (b) JSXQ 3#; (c) XYY A#; (d) SHHM 2#

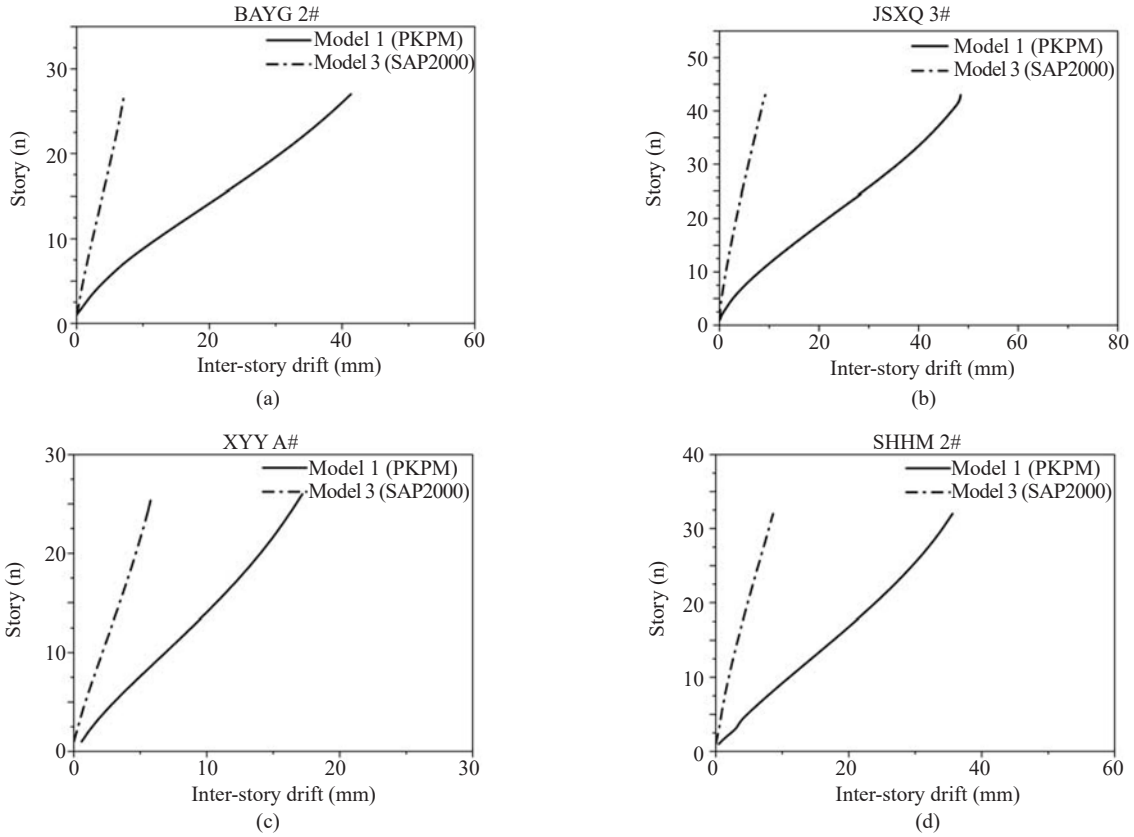

Fig. 15 Story drift of buildings under small earthquakes: (a) BAYG 2#; (b) JSXQ 3#; (c) XYY A#; (d) SHHM 2#

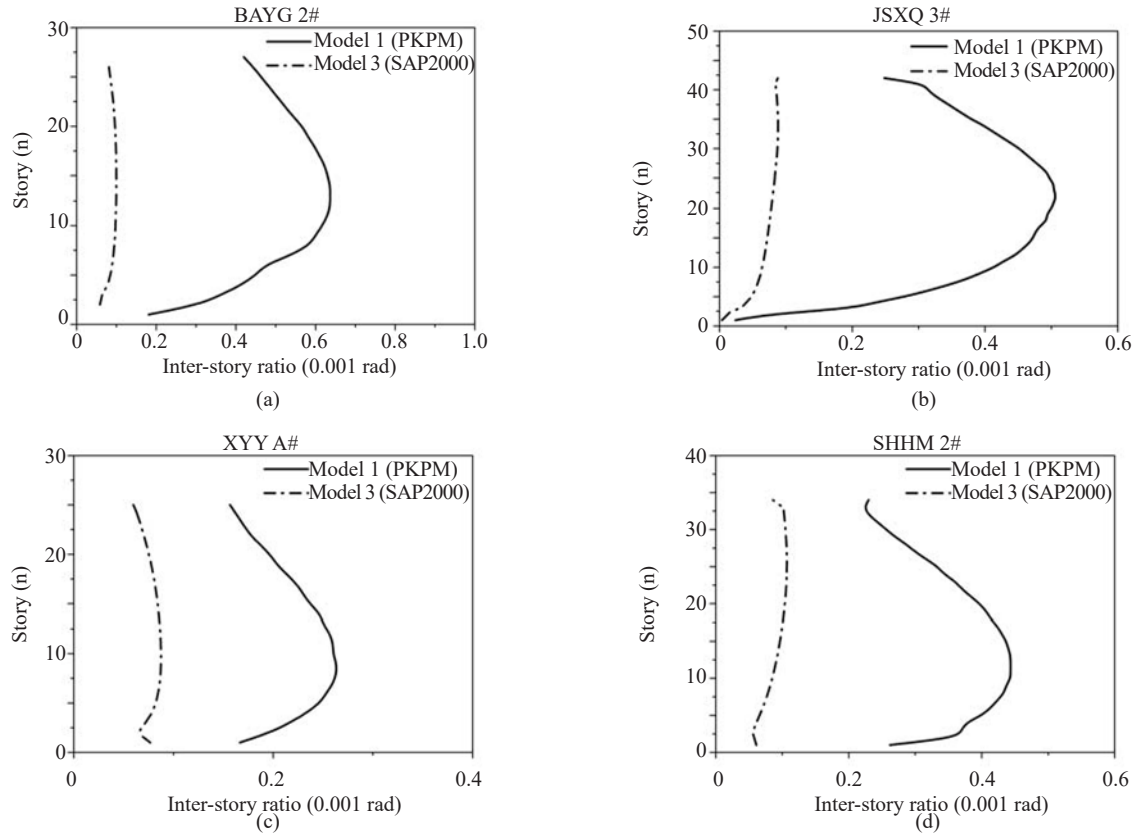

Fig. 16 Inter-story drift ratio under small earthquakes: (a) BAYG 2#; (b) JSXQ 3#; (c) XYY A#; (d) SHHM 2#

6 Nonlinear dynamic analysis results under large earthquakes

6.1 Earthquake records

In nonlinear dynamic analysis, the seismic records should be carefully selected based on the spectrum characteristics, effective magnitude acceleration, and seismic duration (GB 50011-2010, 2010). Three qualified seismic waves in PEER were selected for each high-rise building (refer to Table 5), and the seismic waves were scaled compared with the corresponding target response spectrum (refer to Fig. 17). The seismic waves were applied to FE Models 4 and 5 of four high-rise buildings to conduct nonlinear dynamic analysis.

Table 5 Earthquake records for nonlinear dynamic analysis

Buildings	No.	Record No.	Earthquake records	Time	Mag.	$D_{5\text{-}95}$	V_{30} (m/s)	PGA (cm/s^2)
BAYG 2#	1	RSN66	San Fernando	1971	6.61	23.9	328.09	41.26
	2	RSN300	Irpinia_Italy-02	1980	6.20	20.0	455.93	172.27
	3	RSN906	Big Bear-01	1992	6.46	21.5	328.09	79.07
JSXQ 3#	1	RSN304	Irpinia_Italy-02	1980	6.20	22.1	496.46	20.79
	2	RSN921	Big Bear-01	1992	6.46	23.2	312.47	76.71
	3	RSN937	Big Bear-01	1992	6.46	22.4	416.15	36.11
XYY A#	1	RSN88	San Fernando	1971	6.61	23.6	389.00	151.77
	2	RSN300	Irpinia_Italy-02	1980	6.20	20.0	455.93	172.27
	3	RSN1046	Northridge-01	1994	6.69	22.0	339.60	59.51
SHHM 2#	1	RSN140	Tabas_Iran	1978	7.35	24.2	302.64	102.75
	2	RSN300	Irpinia_Italy-02	1980	6.20	20.0	455.93	172.27
	3	RSN906	Big Bear-01	1992	6.46	21.5	328.09	79.07

Note: $D_{5\text{-}95}$ denotes the significant duration from 5% to 95% of Arias intensity; V_{30} denotes the shear wave velocity in the upper 30 m; and PGA denotes the peak ground acceleration

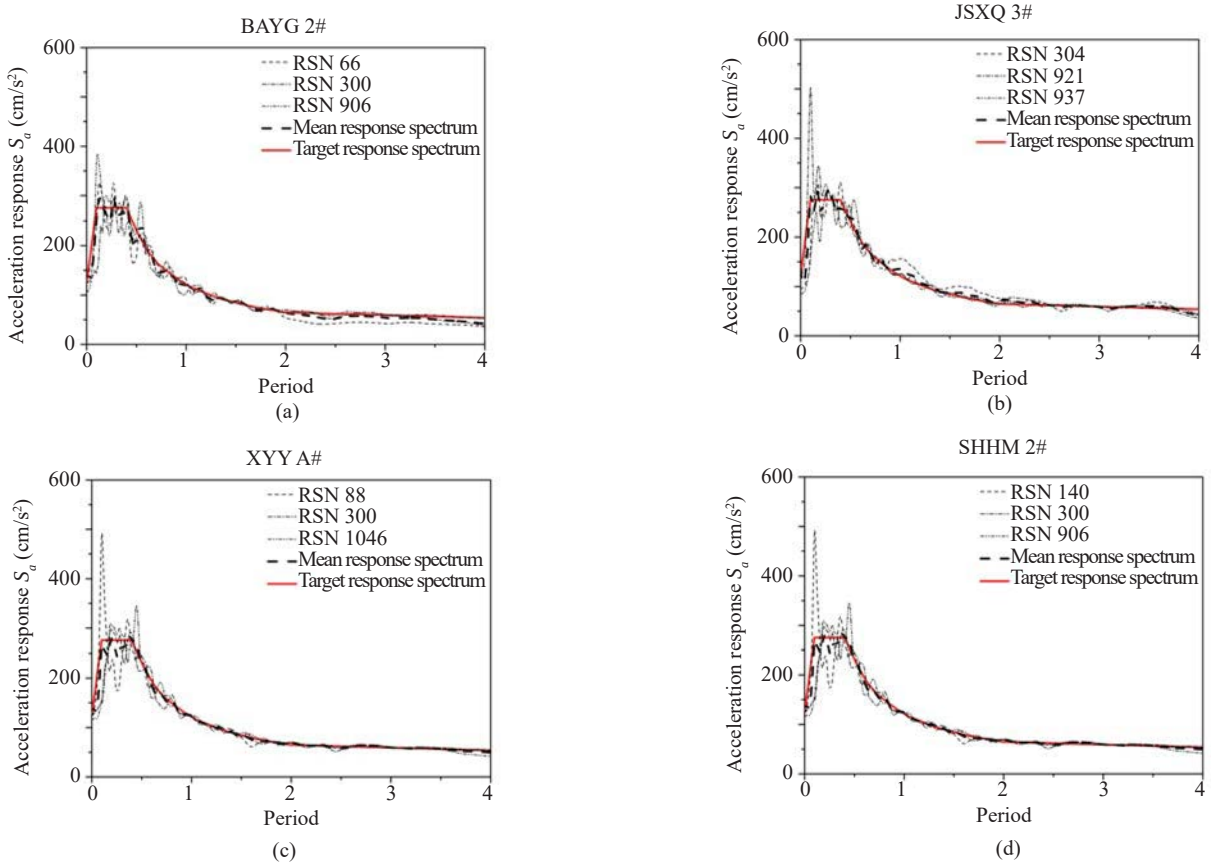

Fig. 17 Seismic response spectra and target response spectra: (a) BAYG 2#; (b) JSXQ 3#; (c) XYY A#; (d) SHHM 2#

6.2 Inter-story shear force

Figure 18 shows the shear force distribution of the column, shear wall, and infill wall. The global structural stiffness was strengthened by the infill wall in Model 5, which increased the inter-story shear force up to 30% to 50%. In Model 4 of BAYG 2#, the inter-story shear force was mainly resisted by the shear wall. On the other hand, the infill wall in Model 5 resisted a large amount of shear force according to the calculation results, which may cause the first shear failure in the infill wall. In the other three shear wall structures, the contribution of the infill wall to the shear resistance was less than that of BAYG 2#. This is because of the specific arrangement of the infill wall or the different structure system used.

6.3 Inter-story drift

Figure 19 shows the story drift of Model 4 and Model 5. Model 5 exhibits 20% to 50% lower story drift due to the contribution of the infill wall to the lateral stiffness. Note that the contribution of the infill wall to the stiffness of the frame-shear wall structure is greater than that of the shear wall structures under large earthquakes.

Figure 20 shows the inter-story drift ratio of Model 4 and Model 5. The drift ratio increases and then decreases from the bottom story to roof story. The maximum inter-story drift ratio occurred at the lower story as the global structural stiffness was increased by the infill wall, and 20% to 50% lower drift ratios were presented in Model 5. The discrepancy of the inter-story drift ratio between the two models for BAYG 2# (i.e., frame-shear wall structure) was greater than that of the other three buildings (i.e., shear wall structure). The inter-story drift ratio of the frame-shear wall structure was less than 0.005 rad, and the ratio of the shear wall structures was less than 0.0025 rad, which satisfied the Chinese design code requirement of 0.01 rad and 0.0083 rad for the frame-shear wall structure and shear wall structure, respectively.

6.4 Seismic energy dissipation

Figure 21 shows the mean energy dissipation estimated by Model 4 and Model 5 for nonlinear behavior of the structures under three selected seismic waves. Compared with Model 4, the enhancement of the structural stiffness by the infill wall in Model 5 increased the energy dissipation of the structures. Regarding the dissipated energy distribution of the structural components, a large amount of seismic energy was dissipated by the flexural behavior of beams of BAYG 2# in Model 4. However, the contribution of the beams to the energy dissipation was significantly decreased, and the infill wall contribution increased in Model 5 with the infill wall. Similar to the previous analysis results, the infill wall dissipated most of the earthquake energy. This result indicates that the infill wall is a more critical

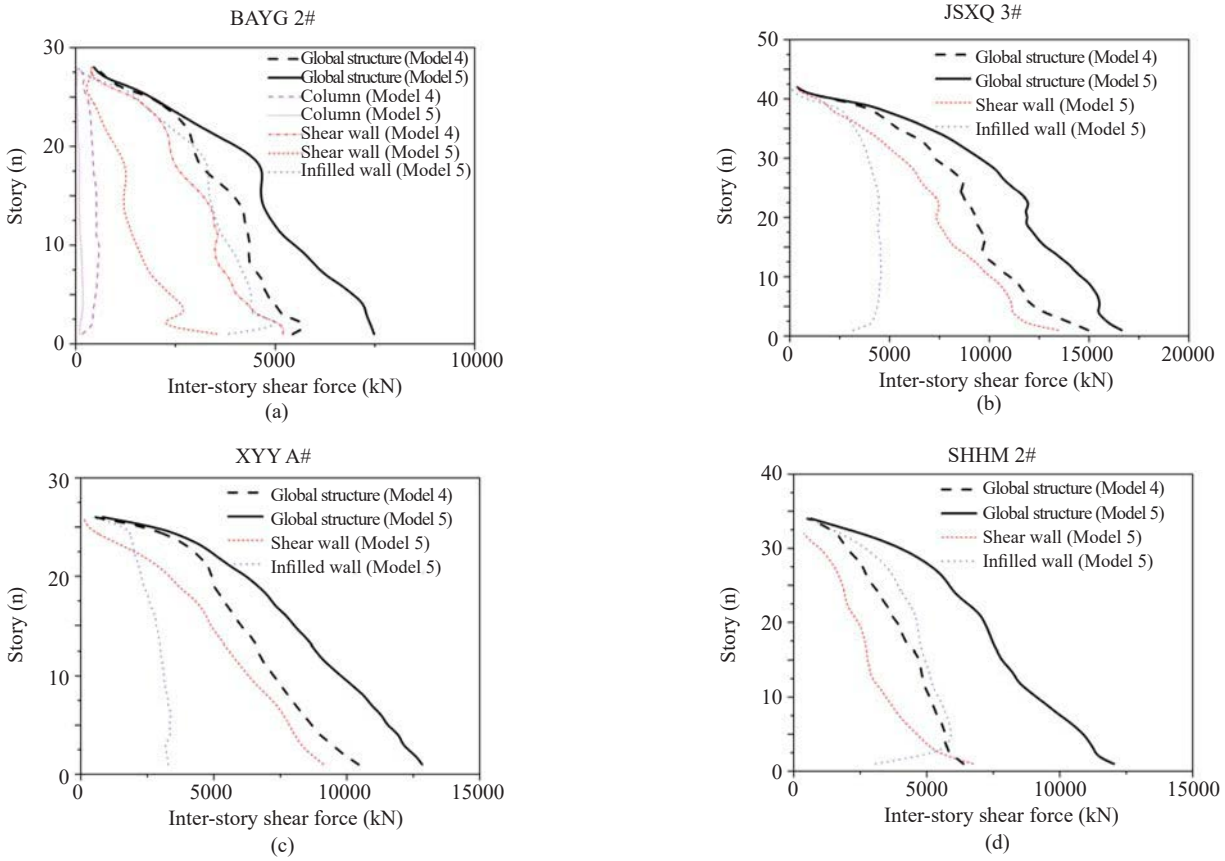

Fig. 18 Shear force distribution of buildings under large earthquakes: (a) BAYG 2#; (b) JSXQ 3#; (c) XYY A#; (d) SHHM 2#

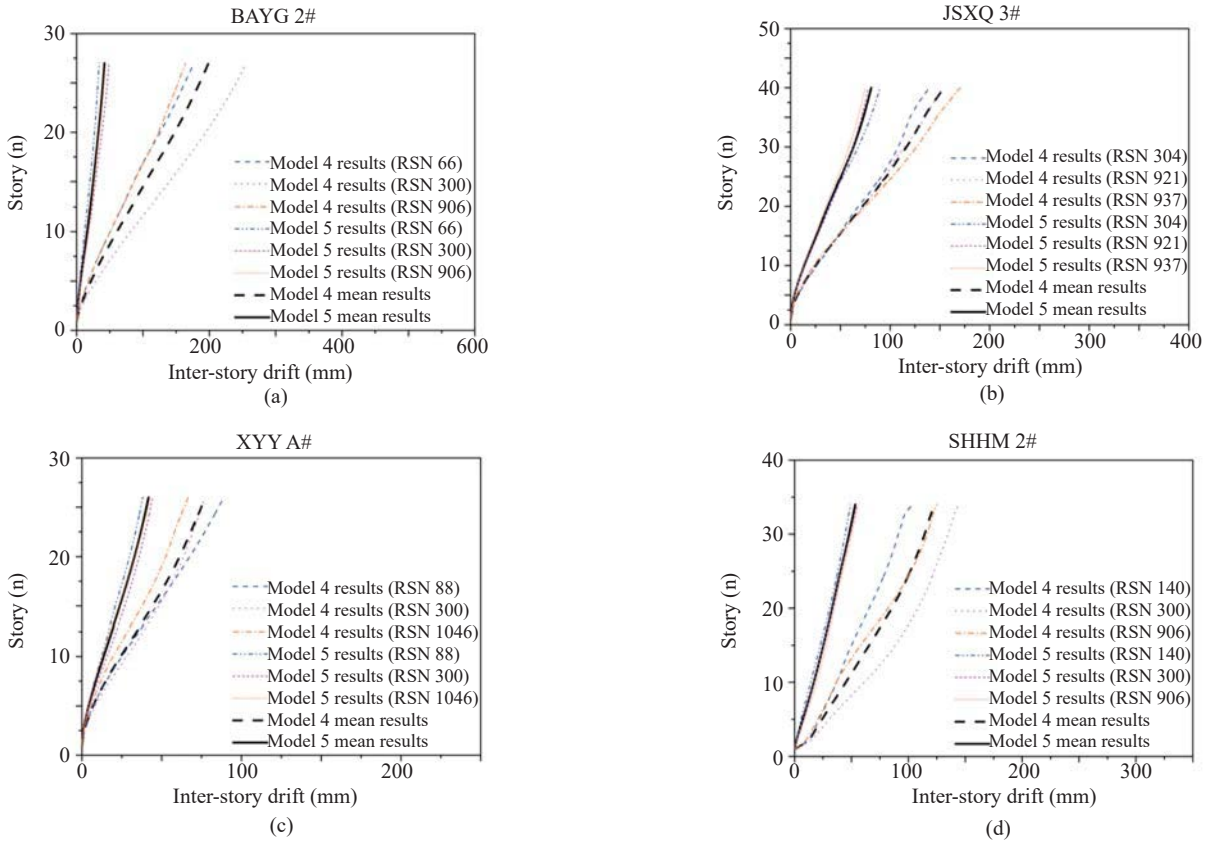

Fig. 19 Story drift of buildings under large earthquakes: (a) BAYG 2#; (b) JSXQ 3#; (c) XYY A#; (d) SHHM 2#

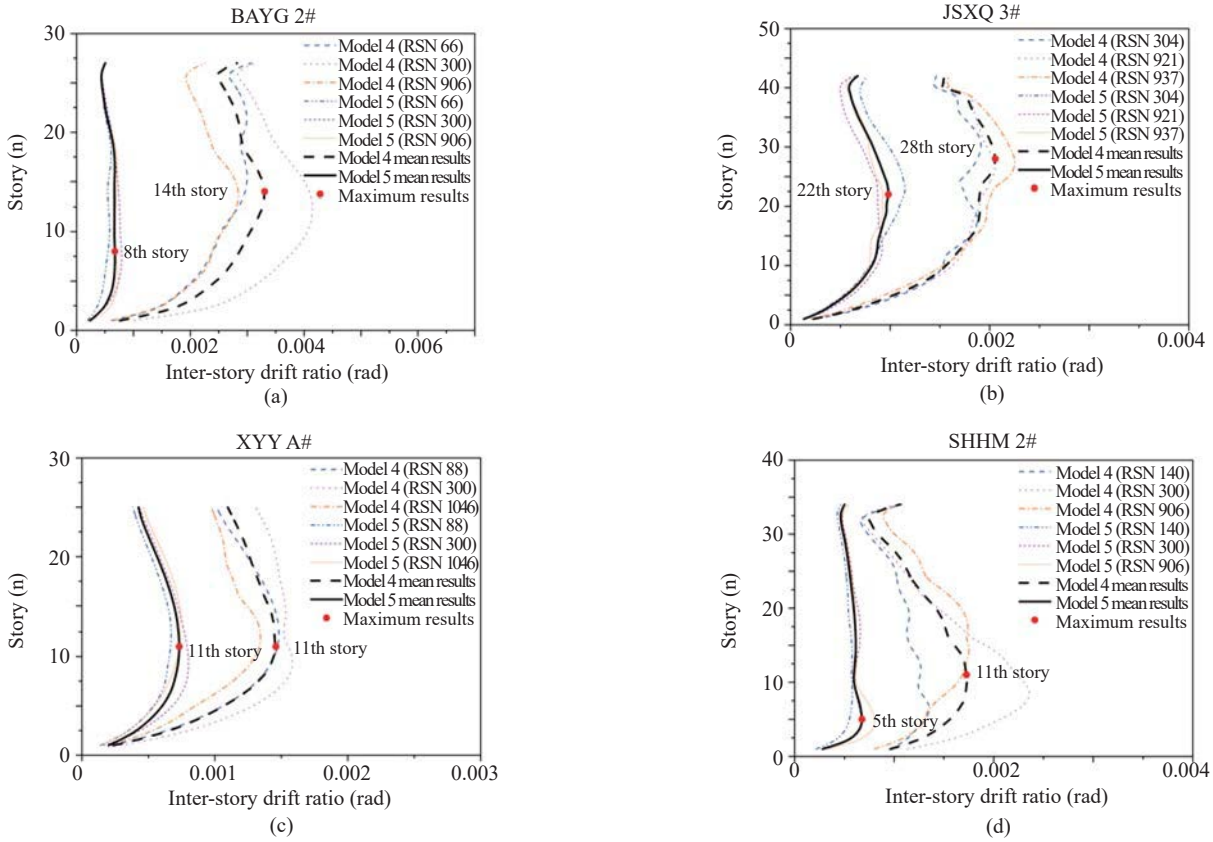

Fig. 20 Inter-story drift ratio under large earthquakes: (a) BAYG 2#; (b) JSXQ 3#; (c) XYY A#; (d) SHHM 2#

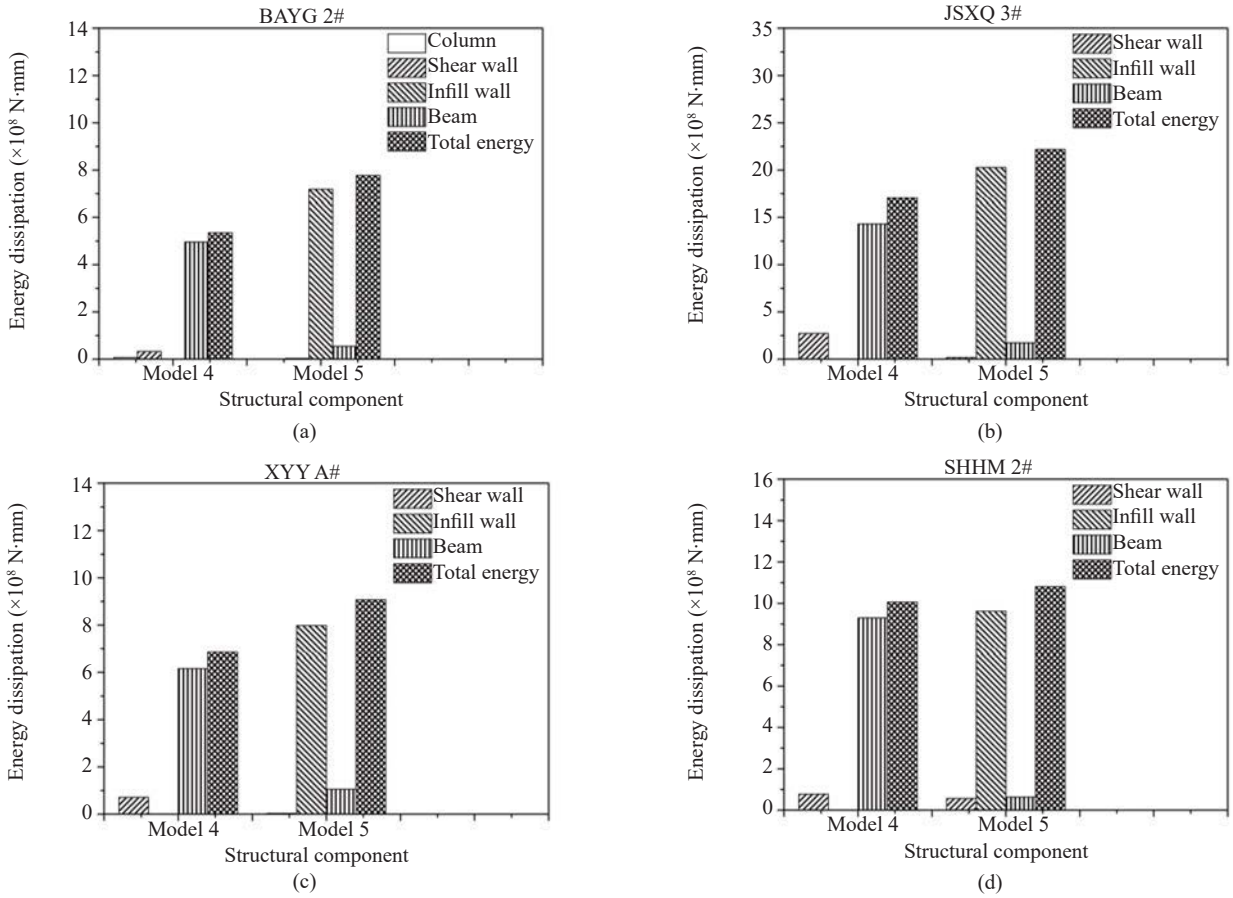

Fig. 21 Comparison of different members under large earthquakes: (a) BAYG 2#; (b) JSXQ 3#; (c) XYY A#; (d) SHHM 2#

member than the other structural members including the beam, column, and shear wall.

Although the FE model of high-rise buildings is calibrated by the natural modal parameters in the linear elastic stage, the nonlinear behavior can be changed, which may differ from the actual situation as a complex process for model calibration is required. Further, the effects of torsion and eccentricity on the structural behavior should be taken into account for the asymmetric structural floor plan condition. An innovative ideology was simply introduced in this study, but further research on nonlinear performance is needed for deeper analysis.

7 Conclusions

In the present study, linear and nonlinear dynamic seismic assessments of high-rise buildings were performed to consider the effect of infill walls. Based on the St-Id ideology, FE models with crossed diagonal struts were built in SAP2000 and PERFORM-3D, and the design parameters of the infill wall were calibrated by comparing the modal periods with the measurements from ambient vibration tests. Two refined FE models were employed to evaluate the seismic performance of the structures: response spectrum analysis under small earthquakes and nonlinear dynamic analysis under large earthquakes. The main conclusions are as follows:

(1) When the contribution of the infill wall to the stiffness is not considered, a large discrepancy of the modal periods between the calculated results of PKPM and measured values was observed. To consider the effect of infill walls in static analysis, the crossed diagonal struts were used in FE models of SAP2000 for four high-rise buildings. The structural dynamic characteristics obtained from ambient vibration tests were applied to calibrate the FE model, and the updated models better predicted the modal periods.

(2) Response spectrum analysis was performed by the calibrated SAP2000 model and PKPM model to evaluate the elastic seismic performance of the structures under small earthquakes. The analysis results showed that compared with the predictions made by the calibrated model of SAP2000, the PKPM model estimated an approximately 50% lower inter-story shear force and 3 to 4 times greater story drift and drift ratio. Thus, the period reduction factor of design codes could be revised to better evaluate the structural performance in the elastic state.

(3) On the basis of the initial elastic modulus calibrated using the periods measured from the actual buildings, the envelope curve with nonlinear

characteristics of infill wall was calculated by the detailed constitutive relationship formulas with the proper elastic modulus. For nonlinear dynamic analysis, the diagonal strut model to describe the effect of infill walls was applied to PERFORM-3D.

(4) Nine earthquake records were selected for nonlinear dynamic analysis of the four high-rise buildings with or without infill walls. The analysis results showed that the maximum inter-story drift ratio of the buildings satisfied the requirement of the design codes. Infill walls significantly contributed to increasing the global lateral stiffness to 30% to 50%, which decreased the inter-story drift ratio to 20% to 50%. Note that the effect of infill walls on the shear demand and drift ratio is significant in the frame-shear wall structure, rather than the shear wall structure.

(5) The use of infill walls increased the energy dissipation capacity in both the frame-shear wall structure and shear wall structure. The contribution of the beam to the energy dissipation decreased, and the contribution of infill walls to energy dissipation increased.

Acknowledgement

The authors sincerely appreciate the funding support provided to this research by the National Key Research and Development Program of China (No. 2016YFC0701400, 2016YFC0701308), the Key Research and Development Program of Hunan Province (No. 2017SK2220), and the National Natural Science Foundation of China (NSFC) (No. 51878264).

References

ASCE (2006), *Minimum Design Loads for Buildings and Other Structures*, Reston, VA.

ASCE (2011), *Structural Identification of Constructed Systems: A State-of-the-art Report*, ASCE-SEI Structural Identification of Constructed Systems Committee, Reston, VA.

Asteris PG, Antoniou ST, Sophianopoulos DS and Chrysostomou CZ (2011), "Mathematical Macromodeling of Infilled Frames: State of the Art," *Journal of Structural Engineering*, **137**(12): 1508–1517.

Asteris PG, Cotsovos DM, Chrysostomou CZ, Mohebkhah A and Al-Chaar GK (2013), "Mathematical Micromodeling of Infilled Frames: State of the Art," *Engineering Structures*, **56**(12): 1905–1921.

Ashok E, Dinesh SV and Dattatreya JK (2015), "Seismic Vulnerability Assessment and Comparison of RC Buildings with and without Infill Using Pushover Analysis," *Journal of Civil Engineering and Environment Technology*, **2**(11): 7–11.

Al-Nimry H, Resheidat M and Qeran S (2015), "Rapid Assessment for Seismic Vulnerability of Low and Medium Rise Infilled RC Frame Buildings," *Earthquake Engineering and Engineering Vibration*, **14**(2): 275–293.

Almeida JP, Tarquini D and Beyer K (2016), "Modelling Approaches for Inelastic Behaviour of RC Walls: Multi-level Assessment and Dependability of Results," *Archives of Computational Methods in Engineering*, **23**(1): 69–100.

Abhijeet VC and Vaibhav VS (2017), "Pushover Analysis of High Rise Building and Outrigger System with or without In-filled Walls," *International Research Journal of Engineering and Technology*, **4**(7): 1439–1445.

Balendra T and Huang X (2003), "Overstrength and Ductility Factors for Steel Frames Designed According to BS 5950," *Journal of Structural Engineering*, **129**(8): 1019–1035.

Brownjohn JM (2003), "Ambient Vibration Studies for System Identification of Tall Buildings," *Earthquake Engineering & Structural Dynamics*, **32**(1): 71–95.

Brownjohn JMW and Pan TC (2008), "Identifying Loading and Response Mechanisms from Ten Years of Performance Monitoring of A Tall Building," *Journal of Performance of Constructed Facilities*, **22**(1): 24–34.

Burak B and Comlekoglu HG (2013), "Effect of Shear Wall Area to Floor Area Ratio on the Seismic Behavior of Reinforced Concrete Buildings," *Journal of Structural Engineering*, **139**(11): 1928–1937.

Carvalho EC and Coelho E (2001), "Seismic Assessment, Strengthening and Repair of Structures," *Ecoest2-Icons Report*, **2**: 3–9.

Catbas FN, Kijewski-Correa T and Aktan AE (2013), "Structural Identification of Constructed Systems: Approaches, Methods, and Technologies for Effective Practice of St-Id," American Society of Civil Engineers (ASCE), Structural Engineering Institute (SEI).

Chaulagain H, Rodrigues H, Spacone E and Varum H (2016), "Seismic Safety Assessment of Existing Masonry Infill Structures in Nepal," *Earthquake Engineering and Engineering Vibration*, **15**(2): 251–268.

Dhakal RP, Pourali A, Tasligedik AS, Yeow T, Baird A, MacRae G, Pampanin S and Palermo A (2016), "Seismic Performance of Nonstructural Components and Contents in Buildings: an Overview of NZ Research," *Earthquake Engineering and Engineering Vibration*, **15**(1): 1–17.

Dolsek M and Fajfar P (2008), "The Effect of Masonry Infills on the Seismic Response of A Four Storey Reinforced Concrete Frame: A Probabilistic Assessment," *Engineering Structures*, **30**(7): 1991–2001.

European Committee for Standardization (2004), *Design of structures for earthquake resistance*, Eurocode 8, CEN, Brussels, Belgium.

Epackachi S, Mirghaderi R and Esmaili O (2012), "Seismic Evaluation of A 56-story Residential Reinforced Concrete High-rise Building Based on Nonlinear Dynamic Time History Analysis," *Structural Design of Tall & Special Buildings*, **21**(4): 233–248.

FEMA 274 (1997), *NEHRP Commentary on the NEHRP*

Guidelines for the Seismic Rehabilitation of Buildings, Federal Emergency Management Agency, Washington.

Fardis MN and Panagiotakos TB (1997), "Seismic Design and Response of Bare and Masonry-infilled Reinforced Concrete Buildings, Part ii: Infilled Structures," *Journal of Earthquake Engineering*, **1**(1): 219–256.

FEMA 306 (1999), *Evaluation of Earthquake Damaged Concrete and Masonry Wall Buildings: Basic Procedures Manual*, Federal Emergency Management Agency, Washington.

Furtado A, Rodrigues H and Arede A (2015), "Modelling of Masonry Infill Walls Participation in the Seismic Behaviour of RC Buildings Using Opensees," *International Journal of Advanced Structural Engineering*, **7**(2): 117–127.

GB 50011-2010 (2010), *Code for Seismic Design of Buildings*, Beijing: China Architecture and Building Press.

Holmes M (1961), "Steel Frames with Brickwork and Concrete Infilling," *Proceedings of the Institution of Civil Engineers*, **19**(4): 473–478.

Henderson RC, Fricke KE, Jones WD, Beavers JE and Bennett RM (2003), "Summary of A Large- and Small-scale Unreinforced Masonry Infill Test Program," *Journal of Structural Engineering*, **129**(12):1667–1675.

Hashmi AK and Madan A (2008), "Damage Forecast for Masonry Infilled Reinforced Concrete Framed Buildings Subjected to Earthquakes in India," *Current Science*, **94**(1): 61–73.

Hans S, Boutin C, Ibraim E and Roussillon P (2010), "In Situ Experiments and Seismic Analysis of Existing Buildings. Part I: Experimental Investigations," *Earthquake Engineering & Structural Dynamics*, **34**(12): 1531–1546.

JGJ 3-2010 (2010), *Technical Specification for Concrete Structures of Tall Building*, Beijing: China Architecture and Building Press.

Kose MM and Karslioglu O (2010), "Effects of Infills on High-rise Buildings: A Case Study," *Structural Design of Tall & Special Buildings*, **18**(8): 907–920.

Kaushik HB, Rai DC and Jain SK (2012), "Code Approaches to Seismic Design of Masonry-Infilled Reinforced Concrete Frames: A State-of-the-Art Review," *Earthquake Spectra*, **22**(4): 961–983.

Liu SC and Yao JTP (1978), "Structural Identification Concept," *Journal of the Structural Division*, **104**(12): 1845–1858.

Li QS and Wu JR (2004), "Full-Scale Measurements and Numerical Evaluation of Wind-induced Vibration of A 63-story Reinforced Concrete Tall Building," *Engineering Structures*, **26**(12): 1779–1794.

Li QS, Wu JR, Liang SG, Xiao YQ and Wong CK (2004), "Correlation of Dynamic Characteristics of A Super-Tall Building from Full-Scale Measurements and Numerical Analysis with Various Finite Element Models," *Earthquake Engineering & Structural Dynamics*, **33**(14): 1311–1336.

Lu HS, Zhao FX (2007), "Site Coefficients Suitable to China Site Category," *Acta Seismologica Sinica*, **29**(1): 67–76.

Luis DD, Laura L and Fabrizio M (2014), "Strength and Stiffness Reduction Factors for Infilled Frames with Openings," *Earthquake Engineering and Engineering Vibration*, **13**(3): 437–454.

Li QS, Zhi LH, Tuan YT, Kao CS and Su SC (2010), "Full-scale Measurements and Analysis of Wind-induced Response of Taipei-101 Tower," *Journal of Building Structures*, **31**(3): 24–31.

Mamun AA and Saatcioglu M (2017), "Seismic Performance Evaluation of Moderately Ductile RC Frame Structures Using Perform-3d," *16th World Conference on Earthquake Engineering*, Santiago Chile.

Mainstone RJ (1971), "Summary of Paper 7360, On the Stiffness and Strengths of Infilled Frames," *Ice Proceedings*, **49**(2): 230.

Manzouri T (1995), "Nonlinear Finite Element Analysis and Experimental Evaluation of Retrofitting Techniques for Unreinforced Masonry Structures," *University of Colorado-Boulder*, USA.

Milheiro J, Rodrigues H and Arede Antonio (2016), "Evaluation of the Contribution of Masonry Infill Panels on the Seismic Behaviour of Two Existing Reinforced Concrete Buildings," *KSCE Journal of Civil Engineering*, **20**(4): 1365–1374.

Mwafy A, Elnashai A, Sigbjornsson R and Salama A (2006), "Significance of Severe Distant and Moderate Close Earthquakes on Design and Behavior of Tall Buildings," *Structural Design of Tall & Special Buildings*, **15**(4): 391–416.

Negro P and Colombo A (1997), "Irregularities Induced by Nonstructural Masonry Panels in Framed Buildings," *Engineering Structures*, **19**(7): 576–585.

NRCC (2005), *National Building Code of Canada*.

Nautiyal P, Singh S, Batham G and Publication I (2013), "A Comparative Study of the Effect of Infill Walls on Seismic Performance of Reinforced Concrete Buildings," *International Journal of Civil Engineering & Technology*, **4**(4): 208–218.

Nwofor TC and Chinwah JG (2014), "Finite Element Modeling of Shear Strength of Infilled Frames with Openings," *International Journal of Engineering & Technology*, **2**(6): 992–1001.

Pacific Earthquake Engineering Research Center, http://ngawest2. berkeley.edu.

Paulay T and Priestley MJN (1992), *Seismic Design of Reinforced Concrete and Masonry Buildings*, Wiley.

Polyakov SV (1960), "On the Interaction between Masonry Filler Walls and Enclosing Frame when Loaded in the Plane of the Wall," *Translations in Earthquake Engineering*, **2**(3): 36–42.

Peeters B (2000), "System Identification and Damage Detection in Civil Engineering," *System Identification and Damage Detection in Civil Engineering*, Katholieke University, Leuven, Belgium.

Smith BS (1962), "Lateral Stiffness of Infilled Frames," *Journal of the Structural Division*, **88**(6): 183–226.

Su RKL, Chandler AM, Sheikh MN and Lam NTK (2005), "Influence of Nonstructural Components on Lateral Stiffness of Tall Buildings," *Structural Design of Tall & Special Buildings*, **14**(2): 143–164.

Shing PB, Stavridis A, Koutromanos I, Willam K, Blackard B, Kyriakides MA and Arnold S (2009), "Seismic Performance of Non-Ductile RC Frames with Brick Infill," *ATC and SEI Conference on Improving the Seismic Performance of Existing Buildings and Other Structures*, 1117–1128.

Sanada Y and Konishi D (2011), "Effects of Nonstructural Brick Infills on An Indonesian Earthquake-Damaged Building," *Procedia Engineering*, **14**: 2077–2085.

Su RKL and Lee CL (2013), "Development of Seismic Fragility Curves for Low-Rise Masonry Infilled Reinforced Concrete Buildings by a Coefficient-Based Method," *Earthquake Engineering and Engineering Vibration*, **12**(2): 319–332.

Tan DX, Zhou Y, Mi ST, Yi WJ, Xie LM and Jiang YZ (2015), "Ambient Vibration Dynamic Test and Finite Element Analysis for High-Rise Buildings," *China Civil Engineering Journal*, **48**(9): 40–50. (in Chinese)

Wu X (2012), "Model Transformation from NosaCAD to ABAQUS and PERFORM-3D and Nonlinear Structure Analysis by These Software," *Building Structure*, **42**(S2): 207–212. (in Chinese)

Wu XH, Sun FT, Lu XL and Qian J (2014), "Nonlinear Time History Analysis of China Pavilion for Expo 2010 Shanghai China," *Structural Design of Tall & Special Buildings*, **23**(10): 721–739.

Xu YL, Chen SW and Zhang RC (2003), "Modal Identification of Di Wang Building under Typhoon York Using the Hilbert-Huang Transform Method," *Structural Design of Tall & Special Buildings*, **12**(1): 21–47.

Zarnic R and Gostic S (1998), "Non-linear Modelling of Masonry Infilled Frames," *Proceedings of 11th European Conference on Earthquake Engineering*, Paris.

Zhang CQ, Zhou Y, Zhou DY and Lu XL (2011), "Study on the Effect of the Infill Walls on the Seismic Performance of a Reinforced Concrete Frame," *Earthquake Engineering and Engineering Vibration*, **10**(4): 507–517.

Zhou Y, Zhou Y, Yi WJ, Tan DX and Mi ST (2017), "Operational Modal Analysis and Rational Finite-Element Model Selection for Ten High-Rise Buildings Based on On-Site Ambient Vibration Measurements," *Journal of Performance of Constructed Facilities*, **31**(5): 04017043.